

Non-standard neutrino interactions and mu-tau reflection symmetry

Jiajun Liao,^{1,*} Newton Nath,^{2,3,†} TseChun Wang,^{1,‡} and Ye-Ling Zhou^{4,§}

¹*School of Physics, Sun Yat-Sen University, Guangzhou 510275, China*

²*Institute of High Energy Physics, Chinese Academy of Sciences, Beijing, 100049, China*

³*School of Physical Sciences, University of Chinese Academy of Sciences, Beijing, 100049, China*

⁴*School of Physics and Astronomy, University of Southampton,
Southampton SO17 1BJ, United Kingdom*

Non-standard interactions (NSI), possible sub-leading effects originating from new physics beyond the Standard Model, may affect the propagation of neutrinos and eventually contributes to measurements of neutrino oscillations. Beside this, $\mu - \tau$ reflection symmetry, naturally predicted by non-Abelian discrete flavour symmetries, has been very successful in explaining the observed leptonic mixing patterns. In this work, we study the combined effect of both. We present a S_4 flavour model with $\mu - \tau$ reflection symmetry realised in both neutrino masses and NSI. Under this formalism, we perform a detailed study for the upcoming neutrino experiments DUNE and T2HK. Our simulation results shows that under the $\mu - \tau$ reflection symmetry, NSI parameters are further constrained and the mass ordering sensitivity is less affected by the presence of NSI.

* Email: liaojiajun@mail.sysu.edu.cn

† Email: newton@ihep.ac.cn

‡ Email: wangzejun@mail.sysu.edu.cn

§ Email: ye-ling.zhou@soton.ac.uk

1. INTRODUCTION

The observation of neutrino oscillations by various experiments using solar, atmospheric, reactor, and accelerator neutrinos indubitably established the existence of neutrino mass, which provides a clear evidence of new physics beyond the Standard Model (SM) [1]. The effective Hamiltonian to describe neutrino oscillation is in general written as

$$H = \frac{1}{2E} (M_\nu M_\nu^\dagger + V) . \quad (1)$$

Here, M_ν is the neutrino mass matrix and V represents the effective potential for neutrino propagating in matter. Considering only the standard matter effect, $V = \text{diag}\{A, 0, 0\}$ with $A = 2\sqrt{2}G_F N_e E$, N_e the electron number density in matter and E the neutrino energy.

Neutrino oscillation data have been inspiring theoretical studies of lepton mixing and mechanisms behind. Traditionally, the observation of maximal atmospheric mixing motivates the notion of the $\mu - \tau$ interchange symmetry, i.e., the permutation between the muon neutrino and the tau neutrino $\nu_\mu \leftrightarrow \nu_\tau$, which predict $\theta_{23} = 45^\circ$ but $\theta_{13} = 0$ [2]. Later, with more precise oscillation data, a critical non-vanishing reactor angle and large CP violation were measured. The so-called the $\mu - \tau$ reflection symmetry, originally proposed in Ref. [3] (for recent review see [4] and the references therein), have been caught more attentions. This symmetry, on the phenomenological side, satisfies $|U_{\mu i}| = |U_{\tau i}|$ (for $i = 1, 2, 3$), which predicts four cases [5]: (a) $\theta_{23} = 45^\circ, \theta_{13} = 0$; (b) $\theta_{23} = 45^\circ, \theta_{12} = 0$; (c) $\theta_{23} = 45^\circ, \theta_{12} = 90^\circ$; (d) $\theta_{23} = 45^\circ, \delta = \pm 90^\circ$. The last case, specifically, $\theta_{23} = 45^\circ, \delta = -90^\circ$, is still in excellent agreement with the latest global analysis of neutrino oscillation data [6].

Various non-Abelian discrete flavour models have been proposed to realise the $\mu - \tau$ reflection symmetry. Among them, the littlest $\mu - \tau$ seesaw model is the most predictive one, where all mixing parameters and the ratio $\Delta m_{21}^2 / \Delta m_{31}^2$ are dependent upon a single RG running parameter [7, 8]. More models have been worked out in the framework of generalised CP symmetry [9, 10]. Combining the $\mu - \tau$ interchange with CP transformation, we arrive at the $\mu - \tau$ reflection transformation,

$$\nu_e \rightarrow \nu_e^c, \quad \nu_\mu \rightarrow \nu_\tau^c, \quad \nu_\tau \rightarrow \nu_\mu^c . \quad (2)$$

Requiring neutrino mass matrix to be invariant under this transformation is equivalent to imposing the following constraint (assuming Majorana neutrinos)

$$X_{\mu\tau}^T M_\nu X_{\mu\tau} = M_\nu^* , \quad (3)$$

where

$$X_{\mu\tau} = \begin{pmatrix} 1 & 0 & 0 \\ 0 & 0 & 1 \\ 0 & 1 & 0 \end{pmatrix} . \quad (4)$$

This immediately leads to

$$M_\nu = \begin{pmatrix} a & b & b^* \\ b & c & d \\ b^* & d & c^* \end{pmatrix}, \quad (5)$$

where a, d are real and b, c are complex. It predicts not just $\theta_{23} = 45^\circ, \delta = \pm 90^\circ$ with non-zero θ_{13} , but also the Majorana phases $\rho, \sigma = 0, 90^\circ$ [11]. Symmetry arguments on how to realise the mass texture in Eq. (5) have been given in based on generalised CP combined with different non-Abelian discrete symmetries, e.g., A_4 [12], S_4 [10, 13], $\Delta(48)$ [14], and $\Delta(96)$ [15]. Examples of explicit model construction can be found in, e.g., [12, 13, 16, 17].

Besides this, new physics beyond the SM may lead to corrections to the effective neutrino interactions through higher-dimensional operators. These operators are often described in the framework of non-standard interactions (NSI). Here, we focus on NSI that can impact the propagation of neutrinos through matter. For neutrinos with kinetic energy around or below GeV scale, they are described by the dimension-6 four-fermion operators of the form [18],

$$\mathcal{L}_{\text{NSI}} = -2\sqrt{2}G_F(\bar{\nu}_\alpha\gamma^\rho P_L\nu_\beta)(\bar{f}\gamma_\rho P_C f)\epsilon_{\alpha\beta}^{fC} + \text{h.c.} \quad (6)$$

where $\epsilon_{\alpha\beta}^{fC}$ represent NSI parameters with $\alpha, \beta = e, \mu, \tau$, $C = L, R$, $f = e, u, d$, and G_F is the Fermi constant.

in the presence of NSI, the effective potential V in Eq. (1) is modified, i.e.,

$$V = A \begin{pmatrix} 1 + \epsilon_{ee} & \epsilon_{e\mu} & \epsilon_{e\tau} \\ \epsilon_{\mu e} & \epsilon_{\mu\mu} & \epsilon_{\mu\tau} \\ \epsilon_{\tau e} & \epsilon_{\tau\mu} & \epsilon_{\tau\tau} \end{pmatrix}, \quad (7)$$

where the 3×3 NSI matrix $\epsilon_{\alpha\beta}$ with $\alpha, \beta = e, \mu, \tau$ is a Hermitian matrix, $\epsilon_{\alpha\beta} = \epsilon_{\beta\alpha}^*$. Next-generation long baseline (LBL) accelerator neutrino oscillation experiments, DUNE [19] and T2HK [20], that aim to do a precision test of standard three neutrino oscillation paradigm will also reach the sensitivity to probe NSI.

In recent times, there have been many interesting studies involving NSI and their impacts on the measurement of standard neutrino oscillation parameters, for detailed reviews see Refs. [21] and the references therein. In [22] authors have addressed various parameter degeneracies between standard and nonstandard interactions for the determination of neutrino mass ordering and the atmospheric mixing angle in case of DUNE and T2HK. In particular, Ref. [23] shows that when $|\epsilon_{e\mu}| = \tan\theta_{23}|\epsilon_{e\tau}|$, a cancellation between leading order terms in the appearance channel probabilities will strongly affect the sensitivities to NSI parameters at T2HK. Also, generalized mass ordering degeneracy has been studied in great detail in [24]. Besides this, some exhaustive analysis in the presence of complex NSI parameters on the determination of the Dirac CP-violating phase have been performed in [25].

Notice that the above mentioned works are mostly based on model independent studies, whereas some model dependent analysis considering heavy charged singlet and/or doublet scalars have been performed in [26]. In these studies, all NSI parameters are assumed to be free complex parameters. Such a large redundancy leads to a difficulty of making definite predictions.

As pointed out in [27], the NSI effects may provide important information to extend our understanding of discrete flavour symmetries. A combined study of the flavour symmetry and NSI can be pursued in the future neutrino experiments. As a result, once the $\mu - \tau$ reflection symmetry is a true symmetry in neutrino mass matrix, one may wonder if NSI also satisfy this symmetry. Furthermore, imposing the $\mu - \tau$ reflection symmetry on the NSI matrix can efficiently reduce the parameter redundancy and satisfy the condition $|\epsilon_{e\mu}| = \tan \theta_{23} |\epsilon_{e\tau}|$ found in [23]. In this paper, we make an attempt to study the importance of NSI for the upcoming LBL neutrino oscillation experiments DUNE and T2HK in the presence of $\mu - \tau$ reflection symmetry. More specifically, we consider NSI matrix that obeys $\mu - \tau$ reflection symmetry and within this framework, the NSI effect has been examined in the context of LBL experiments.

We outline the rest of this work as follows. In Sec. 2, for illustration, we show how to realise $\mu - \tau$ reflection symmetry in both the neutrino mass matrix and NSI matrix in a S_4 flavour model. We follow the technique developed in Ref. [27], which is the first article in the literature which combines NSI with flavour symmetries together. Furthermore, within the S_4 flavour symmetry and the CP symmetry, we show that it is possible to realise NSI matrix that follows $\mu - \tau$ reflection symmetry. In Sec. 3, we perform a phenomenological study of the model both analytically and numerically. Starting from the analysis of the oscillation probabilities, we study the constraints on $\epsilon_{\alpha\beta}$, and then measure the impacts of NSI on the mass ordering sensitivity. We summarise our results in Sec. 4.

2. THE MU-TAU REFLECTION SYMMETRY DRIVEN BY FLAVOUR SYMMETRIES

For illustration, we will construct a flavour model in which the $\mu - \tau$ reflection symmetry is preserved in both the neutrino mass matrix and NSI matrix in the flavour basis. In order to generate the $\mu - \tau$ reflection symmetry in the neutrino mass terms, we introduce the flavour symmetry $S_4 \times Z_4$. We introduce necessary flavon fields which gain VEVs. As a consequence, the flavour symmetry is broken and a non-trivial flavour mixing is obtained. In the electroweak space, we imply the idea of scalar doublet-singlet mixing to generate sizeable NSI [26], where an additional global symmetry, Z_2 , is combined to avoid a myriad of experimental constraints from the charged lepton sector.

We give particle contents of the model in Table I. Three lepton gauge doublets $L =$

$(L_1, L_2, L_3)^T$ are arranged as a triplet $\mathbf{3}$ of S_4 . Three right-handed charged leptons e_R , μ_R and τ_R are singlets of S_4 . Four flavon fields are introduced: φ is a triplet $\mathbf{3}'$ of S_4 to generate charged lepton Yukawa coupling; χ , ζ and ξ are triplet $\mathbf{3}$, doublet $\mathbf{2}$ and singlet $\mathbf{1}$, respectively, to generate the neutrino mass texture. The scalar doublet-singlet mixing is realised by introducing new electroweak doublets η and a charged gauge singlet scalar ϕ^+ , respectively. Here, we arrange η and ϕ^+ as a triplet and a singlet of S_4 , respectively. We discuss how to realise neutrino mass texture and the effective Hamiltonian terms of NSI with the $\mu - \tau$ reflection symmetry, respectively in the following two subsections.

Fields	L	e_R	μ_R	τ_R	H	η	ϕ^+	φ	χ	ζ	ξ
$SU(2)_L$	$\mathbf{2}$	$\mathbf{1}$	$\mathbf{1}$	$\mathbf{1}$	$\mathbf{2}$	$\mathbf{2}$	$\mathbf{1}$	$\mathbf{1}$	$\mathbf{1}$	$\mathbf{1}$	$\mathbf{1}$
$U(1)_Y$	$-\frac{1}{2}$	-1	-1	-1	$+\frac{1}{2}$	$+\frac{1}{2}$	$+1$	0	0	0	0
S_4	$\mathbf{3}$	$\mathbf{1}$	$\mathbf{1}$	$\mathbf{1}'$	$\mathbf{1}$	$\mathbf{3}$	$\mathbf{1}$	$\mathbf{3}'$	$\mathbf{3}$	$\mathbf{2}$	$\mathbf{1}$
Z_4	1	i	-1	$-i$	1	$-i$	$-i$	i	1	1	1
Z_2	$+$	$-$	$+$	$-$	$+$	$-$	$-$	$-$	$+$	$+$	$+$

TABLE I: Particles contents and their assignments in the electroweak gauge symmetry $SU(2)_L \times U(1)_Y$ and flavour symmetry $S_4 \times Z_4$ and an additional global symmetry Z_2 .

2.1. The mu-tau reflection symmetry realised in neutrino mass terms

We first consider the construction of a simplified neutrino mass model. To be invariant in S_4 , the effective Lagrangian terms to generate charged lepton masses and neutrino masses should take the form (c.f. Eq. (A5) of the Appendix)

$$\begin{aligned}
-\mathcal{L} \supset & \bar{L}H \left[\frac{y_e}{\Lambda^3} \begin{pmatrix} \varphi_3^3 - \varphi_2^3 \\ 2\varphi_1^2\varphi_2 - \varphi_2^2\varphi_3 - \varphi_3^2\varphi_1 \\ -2\varphi_1^2\varphi_3 + \varphi_2^2\varphi_1 + \varphi_3^2\varphi_2 \end{pmatrix} e_R + \frac{y_\mu}{\Lambda^2} \begin{pmatrix} \varphi_1^2 - \varphi_2\varphi_3 \\ \varphi_3^2 - \varphi_1\varphi_2 \\ \varphi_2^2 - \varphi_1\varphi_3 \end{pmatrix} \mu_R + \frac{y_\tau}{\Lambda} \begin{pmatrix} \varphi_1 \\ \varphi_2 \\ \varphi_3 \end{pmatrix} \tau_R \right] \\
& + \frac{1}{2\Lambda_{\text{ss}}} \bar{L}\tilde{H} \left[\frac{y_1}{\Lambda} \begin{pmatrix} \xi & 0 & 0 \\ 0 & 0 & \xi \\ 0 & \xi & 0 \end{pmatrix} + \frac{y_2}{\Lambda} \begin{pmatrix} 0 & \zeta_1 & \zeta_2 \\ \zeta_1 & \zeta_2 & 0 \\ \zeta_2 & 0 & \zeta_1 \end{pmatrix} + \frac{y_3}{\Lambda} \begin{pmatrix} 2\chi_1 & -\chi_2 & -\chi_3 \\ -\chi_2 & 2\chi_3 & -\chi_1 \\ -\chi_3 & -\chi_1 & 2\chi_2 \end{pmatrix} \right] H^* L^c + \text{h.c.}, \quad (8)
\end{aligned}$$

where $\bar{L} = \overline{(L_1, L_2, L_3)}$, $\tilde{H} = i\sigma_2 H^*$, Λ is the scale of heavy flavour multiplets decouple and Λ_{ss} is the see-saw scale where heavy mediators (e.g., right-handed neutrinos) decouple. This arrangement can be achieved by arranging additional Z_n charges for flavons [13, 16]. Combining the CP symmetry with the flavour symmetry together and keeping in mind that particles are flavour multiplets in the flavour space, all coefficients are forced to be real [9, 10].

Charged lepton masses are obtained after the flavon φ and the Higgs gain VEVs. Given the VEV for the flavon in the charged lepton sector,

$$\langle\varphi_1\rangle = \langle\varphi_2\rangle = 0, \quad \langle\varphi_3\rangle = v_\varphi, \quad (9)$$

a diagonal charged lepton mass matrix is obtained with diagonal entries given by

$$m_e = \frac{y_e v_\varphi^3}{(2\sqrt{2}G_F)^{1/2}\Lambda^3}, \quad m_\mu = \frac{y_\mu v_\varphi^2}{(2\sqrt{2}G_F)^{1/2}\Lambda^2}, \quad m_\tau = \frac{y_\tau v_\varphi}{(2\sqrt{2}G_F)^{1/2}\Lambda}, \quad (10)$$

where the Higgs VEV $\langle H \rangle = v_H \approx (2\sqrt{2}G_F)^{-1/2} = 174$ GeV has been used. In this case, the three lepton gauge doublets L_1, L_2 and L_3 are identified with the three flavour states $L_e = (\nu_e, e)_L^T, L_\mu = (\nu_\mu, \mu)_L^T, L_\tau = (\nu_\tau, \tau)_L^T$, respectively.

Neutrinos obtain their masses after the flavons χ, ζ, ξ and the Higgs H gain VEVs. Since we assume that the $\mu - \tau$ reflection symmetry is a residual symmetry in the neutrino sector, VEVs of ξ, ζ and χ should be invariant under the relevant transformation, namely,

$$\langle\xi\rangle^* = \langle\xi\rangle, \quad X_{\mu\tau,2} \begin{pmatrix} \langle\zeta_1\rangle \\ \langle\zeta_2\rangle \end{pmatrix}^* = \begin{pmatrix} \langle\zeta_1\rangle \\ \langle\zeta_2\rangle \end{pmatrix}, \quad X_{\mu\tau} \begin{pmatrix} \langle\chi_1\rangle \\ \langle\chi_2\rangle \\ \langle\chi_3\rangle \end{pmatrix}^* = \begin{pmatrix} \langle\chi_1\rangle \\ \langle\chi_2\rangle \\ \langle\chi_3\rangle \end{pmatrix}, \quad (11)$$

where $X_{\mu\tau,2}$ and $X_{\mu\tau}$ are representation-dependent transformation matrix respect to the $\mu - \tau$ reflection,

$$X_{\mu\tau,2} = \begin{pmatrix} 0 & 1 \\ 1 & 0 \end{pmatrix}, \quad X_{\mu\tau} = \begin{pmatrix} 1 & 0 & 0 \\ 0 & 0 & 1 \\ 0 & 1 & 0 \end{pmatrix}. \quad (12)$$

This condition leads to real $\langle\xi\rangle, \langle\chi_1\rangle$ and complex-conjugate pairs $\langle\zeta_1\rangle^* = \langle\zeta_2\rangle, \langle\chi_2\rangle^* = \langle\chi_3\rangle$. We denote them as

$$\begin{aligned} \langle\xi\rangle &= v_1, & \langle\chi_1\rangle &= u_1, \\ \langle\zeta_1\rangle &= v_2 + iv_3, & \langle\zeta_2\rangle &= v_2 - iv_3, \\ \langle\chi_2\rangle &= u_2 + iu_3, & \langle\chi_3\rangle &= u_2 - iu_3, \end{aligned} \quad (13)$$

where v_i and u_i (for $i = 1, 2, 3$) are all real. We then arrive at the neutrino mass matrix in Eq. (5) with

$$\begin{aligned} a &= \frac{y_1 v_1 + 2y_3 u_1}{2\sqrt{2}G_F \Lambda_{ss} \Lambda}, & b &= \frac{y_2 v_2 - y_3 u_2 + i(y_2 v_3 - y_3 u_3)}{2\sqrt{2}G_F \Lambda_{ss} \Lambda}, \\ c &= \frac{y_2 v_2 + 2y_3 u_2 - i(y_2 v_3 + 2y_3 u_3)}{2\sqrt{2}G_F \Lambda_{ss} \Lambda}, & d &= \frac{y_1 v_1 - y_3 u_1}{2\sqrt{2}G_F \Lambda_{ss} \Lambda}. \end{aligned} \quad (14)$$

This is the most general neutrino mass matrix preserving the $\mu - \tau$ reflection symmetry. It is straightforward to check its invariance under the $\mu - \tau$ reflection transformation [11]

$$\nu_e \rightarrow \nu_e^c, \quad \nu_\mu \rightarrow \nu_\tau^c, \quad \nu_\tau \rightarrow \nu_\mu^c. \quad (15)$$

It is equivalent to require

$$X_{\mu\tau}^T M_\nu X_{\mu\tau} = M_\nu^*. \quad (16)$$

This simplified model shows a generic way to achieve flavour mixing with the $\mu - \tau$ reflection symmetry. For an explicit flavour model construction, one should carefully consider how to achieve the required flavon VEVs, and how to avoid the unnecessary higher dimensional operators. In order to solve these problems, supersymmetry and extra fields have to be included, extra Z_n symmetries may be imposed, and UV completion of the effective theory may be considered. For relevant discussions, see e.g., [13, 16, 17]. As a consequence, correlations between oscillation parameters are induced in these models, which can be tested in the future neutrino oscillation experiments. In this paper, we will not consider these parameter correlations.

2.2. The mu-tau reflection symmetry realised in nonstandard interactions

We further discuss how to achieve NSI satisfying the $\mu - \tau$ reflection symmetry. We couple flavons to the NSI mediator charged scalars η and ϕ^+ . Since VEVs of flavons contributing to neutrino masses satisfies the $\mu - \tau$ reflection symmetry, any interactions between these flavons and charged scalars satisfy the $\mu - \tau$ reflection symmetry.

In order to see the behaviour of the $\mu - \tau$ reflection symmetry in NSI, we first consider, the following benchmark Lagrangian terms for illustration,

$$\begin{aligned} -\mathcal{L} \supset & \mu_\eta^2 \eta^\dagger \eta + \mu_\phi^2 \phi^- \phi^+ + \left(f \phi^- \tilde{H}^\dagger (\eta_1 \chi_1 + \eta_2 \chi_3 + \eta_3 \chi_2) + \text{h.c.} \right) \\ & + \lambda (\bar{L}_e \eta_1 + \bar{L}_\mu \eta_2 + \bar{L}_\tau \eta_3) e_R, \end{aligned} \quad (17)$$

where all coefficients are real by imposing CP symmetry. The first row gives rise to charged scalar masses after the SM Higgs obtain the VEV. In the basis $S^+ = (\eta_1^+, \eta_2^+, \eta_3^+, \phi^+)^T$, the charged scalar mass matrix is given by,

$$M_{S^+}^2 = \begin{pmatrix} \mu_\eta^2 & 0 & 0 & f u_1 v_H \\ 0 & \mu_\eta^2 & 0 & f(u_2 + i u_3) v_H \\ 0 & 0 & \mu_\eta^2 & f(u_2 - i u_3) v_H \\ f u_1 v_H & f(u_2 - i u_3) v_H & f(u_2 + i u_3) v_H & \mu_\phi^2 \end{pmatrix}. \quad (18)$$

Here, the Z_2 symmetry is not broken after flavour symmetry breaking and electroweak symmetry breaking. The second row of Eq. (17) gives rise to the interaction of charged scalars, neutrinos and the electron. It is explicitly written out as

$$-\mathcal{L} \supset \overline{(\nu_e, \nu_\mu, \nu_\tau)_L} P_\lambda S^+ e_R \quad (19)$$

where the coefficient matrix P_λ is given by

$$P_\lambda = \lambda \begin{pmatrix} 1 & 0 & 0 & 0 \\ 0 & 1 & 0 & 0 \\ 0 & 0 & 1 & 0 \end{pmatrix} \quad (20)$$

The charged scalars have masses $\gtrsim \mathcal{O}(100)$ GeV. For GeV-scale neutrino beams propagating in the Earth, these scalars can be integrated and dimension-six operators are left,

$$\mathcal{L}_{\text{NSI}} = \overline{(\nu_e, \nu_\mu, \nu_\tau)_L} e_R \left[P_\lambda (M_{S^+}^2)^{-1} P_\lambda^\dagger \right] \overline{e_R} \begin{pmatrix} \nu_e \\ \nu_\mu \\ \nu_\tau \end{pmatrix}_L. \quad (21)$$

With the help of Fierz identity, we express it in the form

$$\mathcal{L}_{\text{NSI}} = -2\sqrt{2}G_F \sum_{\alpha, \beta} \epsilon_{\alpha\beta}^{eR} (\overline{\nu_\alpha} \gamma_\mu P_L \nu_\beta) (\overline{e} \gamma^\mu P_R e), \quad (22)$$

where

$$\epsilon^{eR} = \frac{-1}{4\sqrt{2}G_F} P_\lambda (M_{S^+}^2)^{-1} P_\lambda^\dagger = \begin{pmatrix} \epsilon_{ee} & \epsilon_{e\mu} & \epsilon_{e\mu}^* \\ \epsilon_{e\mu}^* & \epsilon_{\mu\mu} & \epsilon_{\mu\tau} \\ \epsilon_{e\mu} & \epsilon_{\mu\tau}^* & \epsilon_{\mu\mu} \end{pmatrix} \quad (23)$$

with

$$\begin{aligned} \epsilon_{ee} &= 2af^2 (u_2^2 + u_3^2) - 2\sqrt{2}aG_F\mu_\eta^2\mu_\phi^2, & \epsilon_{e\mu} &= -af^2u_1(u_2 - iu_3), \\ \epsilon_{\mu\mu} &= af^2 (u_1^2 + u_2^2 + u_3^2) - 2\sqrt{2}aG_F\mu_\eta^2\mu_\phi^2, & \epsilon_{\mu\tau} &= -af^2(u_2 + iu_3)^2, \end{aligned} \quad (24)$$

where $a^{-1} = 4\sqrt{2}G_F\mu_\eta^2[f^2(u_1^2 + 2u_2^2 + 2u_3^2) - 2\sqrt{2}G_F\mu_\eta^2\mu_\phi^2]$, and the Higgs VEV again has been replaced with $(2\sqrt{2}G_F)^{-1/2}$. In this benchmark, the $\mu - \tau$ reflection symmetry in NSI originates from the contribution of χ to the off-diagonal mass term between η and ϕ^+ . A correlation between NSI parameters, $2\text{Arg}(\epsilon_{e\mu}) + \text{Arg}(\epsilon_{\mu\tau}) = 0$, since only one single source of the $\mu - \tau$ reflection symmetry, i.e. the single coupling with χ , is included. This correlation is easily to be removed by including additional interactions between flavons (ξ , ζ and χ) and charged scalars. Assuming no interactions between the flavon φ and electric-charged scalars, which can be achieved by assuming Z_n charges in the supersymmetry framework, all interactions related to NSI does not induce any source to break the $\mu - \tau$ reflection symmetry, and eventually the $\mu - \tau$ reflection symmetry is always preserved.

This model implies the advantage of using the scalar mixing between electroweak doublets and charged singlets to realise relatively sizeable NSI, $\epsilon_{\alpha\beta} \sim \mathcal{O}(0.1)$. As originally proposed in [26], sizeable NSI require a price of fine-tuning between a large mixing and hierarchical masses for scalars, i.e., the mixing angle around 0.3, a low scalar mass around 100 GeV, and the heavier scalar mass around 10 TeV. Compared with the original model in [26], we extend the gauge doublet η from a flavour singlet to a flavour triplet of S_4 . With the price of fine tuning, NSI $\epsilon_{\alpha\beta} \sim \mathcal{O}(0.1)$ can still be achieved.

3. TESTING MU-TAU REFLECTION SYMMETRY AT DUNE AND T2HK

Here we study the phenomenological consequences of the $\mu - \tau$ reflection symmetry preserved in both the neutrino mass matrix and the NSI matrix. We start our phenomenological study from the analysis on oscillation probabilities with NSI under the $\mu - \tau$ reflection symmetry. In the following, we briefly introduce the experimental setup for experiments, and the analysis details, *e.g.* the true values and priors for oscillation parameters and $\epsilon_{\alpha\beta}$. Before viewing the impact of this symmetry on the mass ordering sensitivity, we investigate the restriction of the $\mu - \tau$ reflection symmetry on the allowed region of $\epsilon_{\alpha\beta}$.

3.1. Neutrino oscillation probabilities

In the framework of the $\mu - \tau$ reflection symmetry, M_ν takes Eq. (5) and $\epsilon_{\alpha\beta}$ satisfy the correlations

$$\epsilon_{e\mu}^* = \epsilon_{e\tau}, \quad \epsilon_{\mu\mu} = \epsilon_{\tau\tau}. \quad (25)$$

Matrices $M_\nu M_\nu^\dagger$ and V , appearing in the Hamiltonian, are expressed in forms of

$$M_\nu M_\nu^\dagger = \begin{pmatrix} \mathbf{a} & \mathbf{b} & \mathbf{b}^* \\ \mathbf{b}^* & \mathbf{c} & \mathbf{d} \\ \mathbf{b} & \mathbf{d}^* & \mathbf{c} \end{pmatrix}, \quad V = A \begin{pmatrix} 1 + \tilde{\epsilon}_{ee} & \epsilon_{e\mu} & \epsilon_{e\mu}^* \\ \epsilon_{e\mu}^* & 0 & \epsilon_{\mu\tau} \\ \epsilon_{e\mu} & \epsilon_{\mu\tau}^* & 0 \end{pmatrix}. \quad (26)$$

with \mathbf{a}, \mathbf{c} are real and \mathbf{b}, \mathbf{d} are complex. We have re-defined V with $\tilde{\epsilon}_{ee} \equiv \epsilon_{ee} - \epsilon_{\tau\tau} = \epsilon_{ee} - \epsilon_{\mu\mu}$ to absorb an overall diagonal phase. Note that in this symmetry based formalism V contains five real free NSI parameters, one real ($\tilde{\epsilon}_{ee}$) and two complex ($\epsilon_{e\mu}, \epsilon_{\mu\tau}$).

The appearance probability for long baseline neutrino oscillation experiments in the presence of NSI is complicated in general [23]. However, under the $\mu - \tau$ reflection symmetry, we can write the appearance probability for the normal ordering (NO) in a simple form, *i.e.*,

$$\begin{aligned} P_{\mu e} &= x^2 f^2 + 2xyfg \cos(\Delta + \delta) + y^2 g^2 \\ &\quad - 4\hat{A}fg|\epsilon_{e\mu}| [x \sin \phi_{e\mu} \sin(\Delta + \delta)] + 4\hat{A}^2 f^2 |\epsilon_{e\mu}|^2 - 4\hat{A}^2 fg |\epsilon_{e\mu}|^2 \sin(2\phi_{e\mu}) \sin \Delta \\ &\quad + \mathcal{O}(s_{13}^2 \epsilon, r\epsilon, s_{13}\epsilon^2, \epsilon^3), \end{aligned} \quad (27)$$

where $\phi_{\alpha\beta} \equiv \text{Arg}(\epsilon_{\alpha\beta})$ and following Ref. [28],

$$\begin{aligned} x &\equiv \sqrt{2}c_{13}s_{13}, \quad y \equiv \sqrt{2}r s_{12}c_{12}, \quad r = |\delta m_{21}^2 / \delta m_{31}^2|, \\ f, \bar{f} &\equiv \frac{\sin[\Delta(1 \mp \hat{A}(1 + \tilde{\epsilon}_{ee}))]}{(1 \mp \hat{A}(1 + \tilde{\epsilon}_{ee}))}, \quad g \equiv \frac{\sin(\hat{A}(1 + \tilde{\epsilon}_{ee})\Delta)}{\hat{A}(1 + \tilde{\epsilon}_{ee})}, \\ \Delta &\equiv \left| \frac{\delta m_{31}^2 L}{4E} \right|, \quad \hat{A} \equiv \left| \frac{A}{\delta m_{31}^2} \right|. \end{aligned} \quad (28)$$

The antineutrino probability $P_{\bar{\mu}e}$, which is given by Eq. (27) with $\delta \rightarrow -\delta$, $\phi_{\alpha\beta} \rightarrow -\phi_{\alpha\beta}$, and $\hat{A} \rightarrow -\hat{A}$ (and hence $f \rightarrow \bar{f}$). For the inverted ordering (IO), $\Delta \rightarrow -\Delta$, $y \rightarrow -y$, $\hat{A} \rightarrow -\hat{A}$ (and hence $f \leftrightarrow -\bar{f}$, and $g \rightarrow -g$).

For small ϵ , we can neglect the y^2 , ϵ^2 and higher order terms in Eq. (27). For $\delta = \pm 90^\circ$ and the NO, we have

$$\begin{aligned} (P_{\mu e})_{\text{NO}} &\simeq x^2 f^2 \mp 2xfg(y \sin \Delta + 2\hat{A}|\epsilon_{e\mu}| \sin \phi_{e\mu} \cos \Delta), \\ (P_{\bar{\mu}e})_{\text{NO}} &\simeq x^2 \bar{f}^2 \pm 2x\bar{f}g(y \sin \Delta + 2\hat{A}|\epsilon_{e\mu}| \sin \phi_{e\mu} \cos \Delta). \end{aligned} \quad (29)$$

For $\delta = \pm 90^\circ$ and the IO, we have

$$\begin{aligned} (P_{\mu e})_{\text{IO}} &\simeq x^2 \bar{f}^2 \mp 2x\bar{f}g(y \sin \Delta - 2\hat{A}|\epsilon_{e\mu}| \sin \phi_{e\mu} \cos \Delta), \\ (P_{\bar{\mu}e})_{\text{IO}} &\simeq x^2 f^2 \pm 2xfg(y \sin \Delta - 2\hat{A}|\epsilon_{e\mu}| \sin \phi_{e\mu} \cos \Delta). \end{aligned} \quad (30)$$

From Eqs. (29) and (30), we see that if $\epsilon_{ee} = 0$ and $\phi_{e\mu} = 0$ or 180° , the differences between the NSI and SM appearance probabilities disappear in both the neutrino and antineutrino modes, which is consistent with the degeneracy between $|\epsilon_{e\mu}|$ and $|\epsilon_{e\tau}|$ found in [23]. Note that for large $|\epsilon_{e\mu}|$, higher order terms cannot be neglected, and the degeneracy is broken.

From Eq. (27), we see that $\epsilon_{\mu\tau}$ does not appear in the appearance probability up to second order in ϵ . Hence, they mainly affect the disappearance channel. Taking ϵ_{ee} , $\epsilon_{e\mu}$ and $\epsilon_{e\tau}$ equal to zero, the disappearance probability can be written as

$$\begin{aligned} P_{\mu\mu} &= 1 - \sin^2 \Delta + rc_{12}^2 \Delta \sin 2\Delta - \frac{s_{13}^2 \sin^2(1 - \hat{A})\Delta}{(1 - \hat{A})^2} \\ &\quad - \frac{s_{13}^2}{(1 - \hat{A})^2} \left[\hat{A}(1 - \hat{A})\Delta \sin 2\Delta + \sin(1 - \hat{A})\Delta \sin(1 + \hat{A})\Delta \right] \\ &\quad - 2\hat{A}|\epsilon_{\mu\tau}| \cos \phi_{\mu\tau} (\Delta \sin 2\Delta) - 2\hat{A}^2 |\epsilon_{\mu\tau}|^2 (2 \cos^2 \phi_{\mu\tau} \Delta^2 \cos 2\Delta + \sin^2 \phi_{\mu\tau} \Delta \sin 2\Delta) \\ &\quad + \mathcal{O}(s_{13}^2 \epsilon, r\epsilon, s_{13} \epsilon^2, \epsilon^3). \end{aligned} \quad (31)$$

The above equation shows that if $\phi_{\mu\tau} = 90$ or 270° , the disappearance probability only depends on the second order in ϵ .

3.2. Experimental and simulation details

In this study, we consider two proposed next-generation superbeam experiments DUNE [19, 29] and T2HK [20]. To perform the numerical simulation of both the experiments, we use the GLOBES packages [30, 31] along with the required auxiliary files presented in Ref. [29] for DUNE and the detector simulation files in Ref. [23] for T2HK. DUNE will utilise existing Neutrinos at the Main Injector (NuMI) beamline design at Fermilab as a neutrino source. The far detector of DUNE will be placed at Sanford Underground Research Facility (SURF)

Parameter	$\theta_{12}/^\circ$	$\theta_{13}/^\circ$	$\theta_{23}/^\circ$	$\delta/^\circ$	$\Delta m_{21}^2/10^{-5}\text{eV}^2$	$\Delta m_{31}^2/10^{-3}\text{eV}^2$
best fit	$33.82^{+0.78}_{-0.76}$	$8.61^{+0.13}_{-0.13}$	$49.6^{+1.0}_{-1.2}$	215^{+40}_{-29}	$7.39^{+0.21}_{-0.2}$	$2.525^{+0.033}_{-0.032}$
3σ Range	31.61 – 36.27	8.22 – 8.99	40.3 – 52.4	125 – 392	6.79 – 8.01	2.47 – 2.625

TABLE II: The best fit and 1σ uncertainty, in the results of NuFit4.0 [6] for normal mass ordering.

in Lead, South Dakota, at a distance of 1300 km (800 mile) and about 1.5 km under the surface from the neutrino source. DUNE collaboration has planned to use four 10-kton liquid argon time-projection chamber (LArTPC) detectors. According to their report, the expected design flux corresponds to 1.07 MW beam power which gives 1.47×10^{21} protons on target (POT) per year for an 80 GeV proton beam energy. In our simulation, we simply consider 40 kton of fiducial mass for the far detector. In addition, the signal and background normalisation uncertainties for appearance and disappearance channels have been adopted from DUNE CDR [29]. We perform our numerical study considering 3.5 years running time in both neutrino and antineutrino modes.

The T2HK experiment [20] will utilise an upgraded J-PARC beam with a power of 1.3 MW, which gives 2.7×10^{21} POT per year for an 30 GeV proton beam energy. They are planning to build a water Cherenkov (WC) detector, which is located 295 km away from the source. Making the detector 2.5° off-axis allows it to measure a narrow band beam with a peak energy around 0.6 GeV. Here we consider the 2TankHK-staged design proposed in the HK design report [20]. We assume one tank will take data alone for the first six years, whereas a second tank will be added for another four years. Each tank will have 0.19 Mton fiducial mass with 40% photocoverage. While performing the numerical analysis, we take 2.5 years running time in neutrino modes and 7.5 years running time in anti-neutrino modes, i.e., 1 : 3 ratio out of the total runtime.

To incorporate NSI, we use the GLoBES extension file `snu.c` as has been presented in Refs. [32, 33]. To implement the $\mu - \tau$ reflection symmetry, we directly impose the form Eq. (26) on the matter potential in `snu.c`. We set the true parameter values of NSI as zero, whereas the test parameter ranges of NSI have been considered from [21].

Except for the value of δ and θ_{23} , we use NuFit4.0 best-fit results for the true values [6], as shown in Tab. II. We fix the value θ_{13} at the true value, as we have checked it does not make a great impact on the measurement on NSI parameters. We also fix θ_{12} and Δm_{21}^2 at the true values as these two parameters do not enter to the neutrino oscillations of DUNE and T2HK. We vary Δm_{31}^2 within a Gaussian prior with the true value and the width which are the best fit and the 1σ uncertainty of NuFit4.0 results. In addition, we consider two orderings: for normal (inverse) mass ordering, the central value and the 1σ relative width of the Δm_{31}^2 prior are 2.525 eV^2 (-2.586 eV^2) and 1.3% (1.3%), respectively. We do not

include any other priors. Furthermore, we vary the phases $\phi_{e\mu}$ and $\phi_{\mu\tau}$ in the range $[0, 2\pi)$. Note that the $\mu - \tau$ reflection symmetry supports the phases $\phi_{e\mu}, \phi_{\mu\tau} \neq 0, \pi$. Finally, we do not consider the LMA-dark solution that is allowed by the generalized mass ordering degeneracy [24], since it is difficult to achieve $\epsilon_{\alpha\beta} \sim \mathcal{O}(1)$ in the flavor symmetrical models.

3.3. Constraints on NSI parameters

We first study the impact of imposing the $\mu - \tau$ reflection symmetry on the constraints on NSI parameters at next-generation superbeam experiments. In Fig. 1, we present the allowed parameter region on the $|\epsilon_{e\mu}| - |\epsilon_{e\tau}|$ plane without restricting the $\mu - \tau$ reflection symmetry on $\epsilon_{\alpha\beta}$ for DUNE (solid) and the synergy of DUNE and T2HK (dashed). Gray, orange and black curves represent 1σ , 2σ , and 3σ contours, respectively. The tendency of contours leaves away from $|\epsilon_{e\mu}| = |\epsilon_{e\tau}|$, because of the contribution from the higher-order term in $P(\nu_\mu \rightarrow \nu_e)$ and $P(\bar{\nu}_\mu \rightarrow \bar{\nu}_e)$. Along with $|\epsilon_{e\mu}| = |\epsilon_{e\tau}|$, the bounds at 1σ , 2σ and 3σ are ~ 0.125 , ~ 0.16 , and ~ 0.19 , respectively. Obviously, this shows that when we impose the restriction of the $\mu - \tau$ reflection symmetry on NSI, the uncertainty of $|\epsilon_{e\mu}|$ and $|\epsilon_{e\tau}|$ is much reduced. We see a deficit for all contours. For example, for the 3σ contour for DUNE, the discontinuity appears around $|\epsilon_{e\mu}| \sim 0.25$ and $|\epsilon_{e\tau}| \sim 0.5$. This is because the flipping of the sign of Δm_{31}^2 .

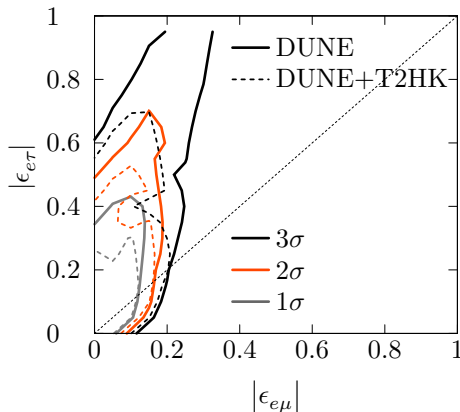


FIG. 1: The 1σ (gray), 2σ (red), and 3σ (black) contours on the $|\epsilon_{e\mu}| - |\epsilon_{e\tau}|$ plane without restricting the $\mu - \tau$ symmetry.

In Fig. 2, we discuss on the scenario in the presence of the $\mu - \tau$ reflection symmetry on NSI. We show 1σ (gray), 2σ (red), and 3σ (black) contours on $\tilde{\epsilon}_{ee} - |\epsilon_{e\mu}|$ (left), $|\epsilon_{\mu\tau}| - |\epsilon_{e\mu}|$ (right) planes for DUNE (solid) and the combination of DUNE and T2HK (dashed). We see a correlation between $|\epsilon_{e\mu}|$ and $|\epsilon_{\mu\tau}|$. This is because of the flipping of $\text{sign}(\Delta m_{31}^2)$. In the other panel, we see that there is a dip on top of solid curves. This feature can be removed by

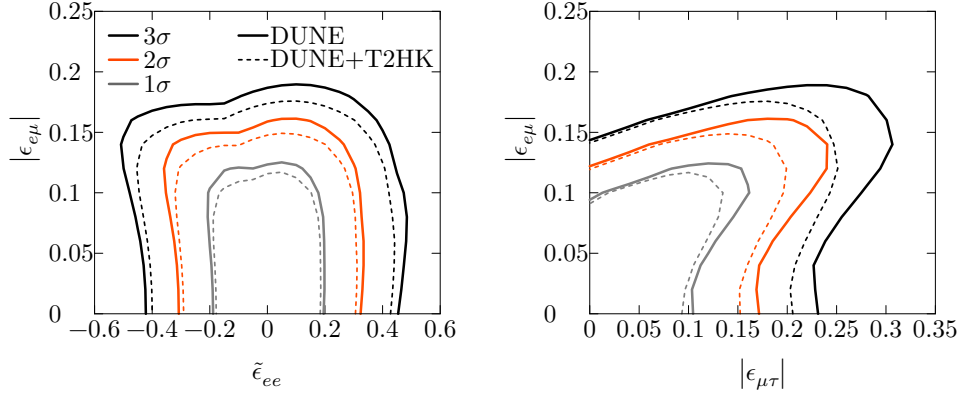


FIG. 2: The 1σ (gray), 2σ (red), and 3σ (black) contours on $\tilde{\epsilon}_{ee} - |\epsilon_{e\mu}|$ (upper) and $|\epsilon_{\mu\tau}| - |\epsilon_{e\mu}|$ (upper) for DUNE (solid) and the combination of DUNE and T2HK (dashed). We vary phases $\phi_{e\mu}$ and $\phi_{\mu\tau}$ in $(0, 2\pi)$. Δm_{31}^2 is allowed to be varied by within a Gaussian prior with a 1σ relative width of $\sim 1.25\%$. Two mass orderings are considered. No other priors are used.

Parameters	1σ w/o $\mu - \tau$	1σ w/ $\mu - \tau$
$\tilde{\epsilon}_{ee}$	$[-2.5, 1.2]$	$[-0.13, 0.13]$
$ \epsilon_{e\mu} $	$[0, 0.12]$	$[0, 0.1]$
$ \epsilon_{e\tau} $	$[0, 0.3]$	$[0, 0.1]$
$ \epsilon_{\mu\tau} $	$[0, 0.2]$	$[0, 0.12]$

TABLE III: The comparison of the constraints on NSI parameters between cases with (w/) and without (w/o) the restriction of the $\mu - \tau$ reflection symmetry for DUNE.

including T2HK data. Taking about the size of constraints, though T2HK is not sensitive for measuring NSI parameters, including its data significantly improves the $|\epsilon_{\mu\tau}|$ measurement, for which T2HK data can reduce the size of the uncertainty by $\sim 20\%$. The improvement on the other parameters is weaker. We note that the size of uncertainties is reduced once the $\mu - \tau$ reflection symmetry is preserved in NSI. We compare the 1σ constraints between scenarios with and without the $\mu - \tau$ reflection symmetry for DUNE in Tab. III. We see the improvement of the precision of $\tilde{\epsilon}_{ee}$ and $|\epsilon_{\mu\tau}|$ measurements, which is not only because of the fact that the number of degrees of freedom is reduced by imposing the $\mu - \tau$ reflection symmetry in the neutrino-mass matrix and NSI, but also the size of the allowed region for $|\epsilon_{e\tau}|$ is largely shrunk down.

3.4. Impact on neutrino mass ordering sensitivity

The main goals of next-generation neutrino oscillation experiments are to measure the Dirac CP phase δ and to determine the neutrino mass ordering and the octant of θ_{23} [19]. Since the $\mu - \tau$ reflection symmetry is preserved in both the neutrino mass matrix and NSI matrix in our formalism, $\theta_{23} = 45^\circ$ and $\delta = \pm 90^\circ$ will be measured by future neutrino oscillation experiments even in the presence of NSI. We find that the wrong sign of δ can be excluded at more than 5σ CL at DUNE and T2HK. Hence, here we fix $\delta = -90^\circ$ which is favored by the latest global analysis of neutrino oscillation data [6], and only focus on the study of the impact of NSI on the determination of mass ordering sensitivity at DUNE and T2HK within this formalism.

We first examine the potential of both experiments to measure the mass ordering in the presence of standard matter interactions as shown in Fig. 3. The combined potential of both experiments are also investigated. The solid green curve shows the ordering χ^2 for DUNE, the dashed-dotted brown curve represents the same for T2HK. The combined potential of DUNE and T2HK are shown by the dotted green curve. We also mark the 3σ , 5σ significance levels by the solid and dotted black horizontal lines, respectively. Our result is consistent with that in Ref. [34]. We notice that DUNE and T2HK can achieve a maximum ordering sensitivity of around $\sqrt{\chi^2} \sim 20$ and 5 significance levels, respectively, around the true value of the Dirac CP-violating phase $\delta = -90^\circ$, respectively. Though the mass ordering sensitivity for T2HK is not good as DUNE, we see an improvement by combining two sets of data. Thus, in what follows we discuss about the DUNE and the combination of DUNE+T2HK.

To investigate the impact of NSI on the determination of neutrino mass ordering under the adopted formalism, we present our results in the left panel of Fig. 4. For simplicity, we first discuss our results for non-zero $\epsilon_{e\mu}, \epsilon_{e\tau}$, whereas the remaining NSI (i.e., $\tilde{\epsilon}_{ee}, \epsilon_{\mu\tau}$) have been fixed at zero. We show our results for the DUNE (DUNE+T2HK) using solid curves (dotted curves). The orange curves show our results in the presence of the symmetry, whereas the blue curves represent the same but in absence of the symmetry. Note that for $\epsilon_{e\mu} \neq \epsilon_{e\tau}^*$ curves, the parameter $\epsilon_{e\tau}$ has been marginalised in our analysis. In the case of DUNE, we notice that the mass ordering sensitivity does not get much affected for $\epsilon_{e\mu} \lesssim 0.15$ when the NSI parameters respect the symmetry over the whole parameter space (see solid orange curve). Including T2HK data slightly improves the sensitivity. On the other hand, noticeably sizeable impact has been observed when the NSI parameters fail to respect the symmetry (i.e. for $\epsilon_{e\mu} \neq \epsilon_{e\tau}^*$), which we show by the solid blue curve for the DUNE (see figure levels for details). The sensitivity curve gets severely affected for $\epsilon_{e\mu} \lesssim 0.15$ as can be seen from the solid blue curve. The impact of NSI on the mass ordering sensitivity is not reduced by including T2HK data. In the right panel of Fig. 4, we also demonstrate the

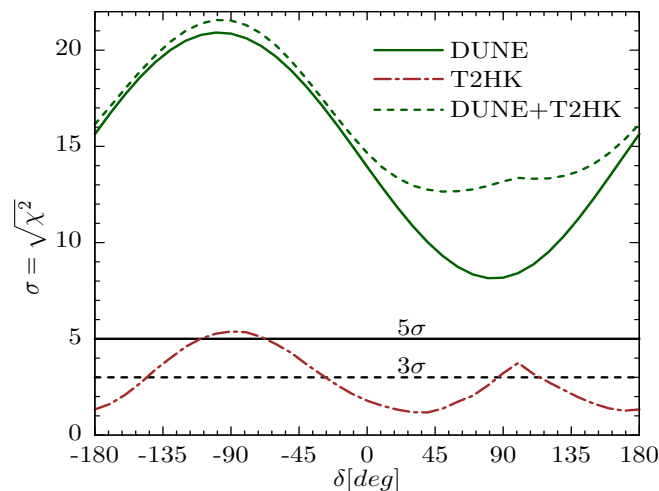


FIG. 3: Mass ordering sensitivity in the presence of standard matter interactions. Here, green solid (brown dashed-dotted) curve represents the χ^2 sensitivity for DUNE (T2HK), whereas their combined analysis are shown by the green dotted curve.

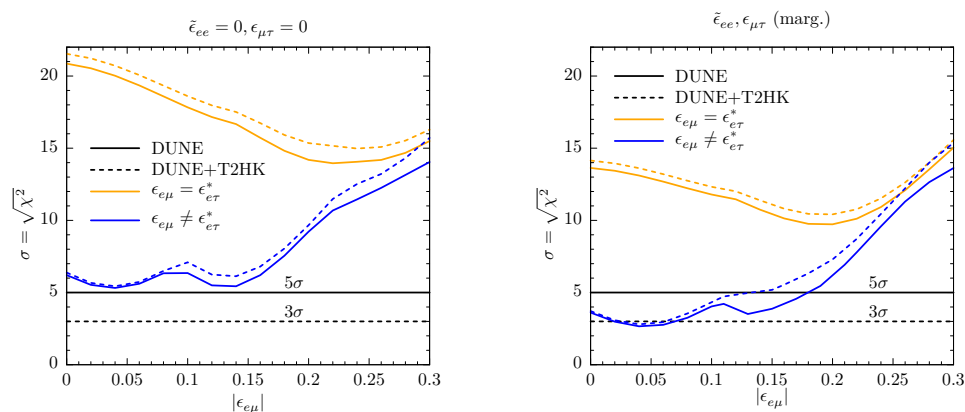


FIG. 4: Left: mass ordering χ^2 vs $\epsilon_{e\mu}$ for $\tilde{\epsilon}_{ee} = 0, \epsilon_{\mu\tau} = 0$ and $\delta = -90^\circ$, where solid (dashed) curve shows the sensitivity level for DUNE (DUNE+T2HK). Also, the orange curves depict our results within the symmetry, whereas in absence of the symmetry are shown by the blue curves. Right: Same as the left, except for values of $\tilde{\epsilon}_{ee}$ and $\epsilon_{\mu\tau}$ marginalised over (marg.).

mass ordering χ^2 similar to the left, but for the most general picture, i.e., in the presence of all the NSI parameters ($\tilde{\epsilon}_{ee}, \epsilon_{e\mu}, \epsilon_{\mu\tau}$) within the symmetry framework. We see the same behaviour of the mass ordering sensitivity in the right panel of Fig. 4, i.e., by comparing the sensitivity curves in the left of with the right panel. However, we notice the stronger impact of varying $\tilde{\epsilon}_{ee}$ and $\epsilon_{\mu\tau}$ on the mass ordering sensitivity with the $\mu - \tau$ reflection symmetry.

4. SUMMARY

The $\mu - \tau$ reflection symmetry which predicts the maximal value of the atmospheric mixing angle as well as the Dirac CP-violating phase are in well agreement with the latest neutrino oscillation data. In this work, we explore the possibility of embedding the $\mu - \tau$ reflection symmetry in the NSI matrix and study its importance for the determination of neutrino mass ordering in case of DUNE and T2HK.

We present an S_4 flavour model, with the $\mu - \tau$ reflection symmetry realised in both neutrino mass matrix and NSI matrix. In this model, The sizeable NSI effects originate from the mediator of scalar doublet-singlet mixing. The essential to achieve the $\mu - \tau$ reflection symmetry is the introduction of flavon fields and assuming the vacuum satisfies the symmetry. By coupling the flavons to neutrinos, the $\mu - \tau$ reflection symmetry in neutrino mass matrix is realised. By coupling the flavons to the scalar mediators, that in the NSI matrix is achieved. The model provides a very generic way to construct NSI with the $\mu - \tau$ reflection symmetry.

We find that imposing the $\mu - \tau$ reflection symmetry improves the constraints on NSI parameters. In particular, the constraint to $\tilde{\epsilon}_{ee}$ is improved most, its allowed regime is improved from $[-2.5, 1.2]$ (without the $\mu - \tau$ reflection symmetry) to $[-0.13, -0.13]$ (within the $\mu - \tau$ reflection symmetry). It is not just because of the reduced numbers of NSI parameters, but also due to the fact that the allowed region for $\epsilon_{e\tau}$ is reduced. This exactly points out that NSI under this scenario are much more testable with the upcoming neutrino oscillation experiments.

We also study the impact of NSI on the mass ordering sensitivity. Assuming $\tilde{\epsilon}_{ee} = \epsilon_{\mu\tau} = 0$, we find that in the presence of the $\mu - \tau$ reflection symmetry, DUNE alone can reach almost 14σ mass ordering sensitivity. However, the mass ordering sensitivity gets compromised in absence of the concerned symmetry as presented in Fig. 4. We find slightly better sensitivity for DUNE+T2HK. Considering the most general scenario under the $\mu - \tau$ reflection symmetry, we find that DUNE can achieve more than 10σ sensitivity, whereas the combined analysis of DUNE+T2HK data can give relatively better sensitivity than DUNE.

In summary, the existence of the $\mu - \tau$ reflection symmetry in the neutrino mass matrix and matter effect NSI is attractive in both theoretical and phenomenological points of view. It is naturally realised in the framework of flavour symmetries, and is consistent with the current data. Furthermore, once the $\mu - \tau$ reflection symmetry is the true symmetry behind, the testability of NSI is enhanced, and the impact of NSI on the mass ordering sensitivity is reduced.

ACKNOWLEDGMENTS

NN thanks Prof. Zhi-zhong Xing for an opportunity to visit Sun Yat-sen University, Guangzhou and also acknowledges their warm hospitality, where the work has been initiated. JL is supported in part by National Natural Science Foundation of China under grant No. 11905299. NN is supported in part by the National Natural Science Foundation of China under grant No. 11775231. TCW is supported in part by the National Natural Science Foundation of China under Grant No. 11505301 and No. 11881240247. YLZ acknowledges the STFC Consolidated Grant ST/L000296/1 and the European Union's Horizon 2020 Research and Innovation programme under Marie Skłodowska-Curie grant agreements Elusives ITN No. 674896 and InvisiblesPlus RISE No. 690575.

Appendix A: Group theory of S_4

S_4 is the permutation group of 4 objects. Its three generators S , T and U satisfying the equalities $T^3 = S^2 = U^2 = (ST)^3 = (SU)^2 = (TU)^2 = 1$, from which $(STU)^4 = 1$ is automatically obtained. The minimal number of generators of S_4 is actually two [35, 36]. However, we follow the presentation in [37] to emphasise the Z_2 residual symmetries generated by S and U , respectively. S_4 contains 5 irreducible representations (irreps), $\mathbf{1}$, $\mathbf{1}'$, $\mathbf{2}$, $\mathbf{3}$ and $\mathbf{3}'$. The Kronecker products between different irreps can be easily obtained:

$$\begin{aligned} \mathbf{1} \otimes \mathbf{r} &= \mathbf{r}, \quad \mathbf{1}' \otimes \mathbf{1}' = \mathbf{1}, \quad \mathbf{1}' \otimes \mathbf{2} = \mathbf{2}, \quad \mathbf{1}' \otimes \mathbf{3} = \mathbf{3}', \quad \mathbf{1}' \otimes \mathbf{3}' = \mathbf{3}, \quad \mathbf{2} \otimes \mathbf{2} = \mathbf{1} \oplus \mathbf{1}' \oplus \mathbf{2}, \\ \mathbf{2} \otimes \mathbf{3} &= \mathbf{2} \otimes \mathbf{3}' = \mathbf{3} \oplus \mathbf{3}', \quad \mathbf{3} \otimes \mathbf{3} = \mathbf{3}' \otimes \mathbf{3}' = \mathbf{1} \oplus \mathbf{2} \oplus \mathbf{3} \oplus \mathbf{3}', \quad \mathbf{3} \otimes \mathbf{3}' = \mathbf{1}' \oplus \mathbf{2} \oplus \mathbf{3} \oplus \mathbf{3}', \end{aligned} \quad (\text{A1})$$

where \mathbf{r} represents any irrep of S_4 . Throughout this paper, we work in the basis where the generator T diagonal. Generators of S_4 in different irreps are listed in Table IV. In this basis, once we arrange $a = (a_1, a_2, a_3)^T$ as a triplet $\mathbf{3}$ (or $\mathbf{3}'$) of S_4 , $\tilde{a} = (a_1^*, a_3^*, a_2^*)^T$, instead of $(a_1^*, a_2^*, a_3^*)^T$, transforms as a triplet of S_4 .

Given two triplets $a = (a_1, a_2, a_3)^T$ and $b = (b_1, b_2, b_3)^T$, irreducible representations for products of a and b are given by

$$\begin{aligned} (ab)_{\mathbf{1}} &= a_1 b_1 + a_2 b_3 + a_3 b_2, \\ (ab)_{\mathbf{2}} &= (a_2 b_2 + a_1 b_3 + a_3 b_1, \quad a_3 b_3 + a_1 b_2 + a_2 b_1)^T, \\ (ab)_{\mathbf{3}} &= (2a_1 b_1 - a_2 b_3 - a_3 b_2, \quad 2a_3 b_3 - a_1 b_2 - a_2 b_1, \quad 2a_2 b_2 - a_3 b_1 - a_1 b_3)^T, \\ (ab)_{\mathbf{3}'} &= (a_2 b_3 - a_3 b_2, \quad a_1 b_2 - a_2 b_1, \quad a_3 b_1 - a_1 b_3)^T, \end{aligned} \quad (\text{A2})$$

	T	S	U
$\mathbf{1}$	1	1	1
$\mathbf{1}'$	1	1	-1
$\mathbf{2}$	$\begin{pmatrix} \omega & 0 \\ 0 & \omega^2 \end{pmatrix}$	$\begin{pmatrix} 1 & 0 \\ 0 & 1 \end{pmatrix}$	$\begin{pmatrix} 0 & 1 \\ 1 & 0 \end{pmatrix}$
$\mathbf{3}$	$\begin{pmatrix} 1 & 0 & 0 \\ 0 & \omega^2 & 0 \\ 0 & 0 & \omega \end{pmatrix}$	$\frac{1}{3} \begin{pmatrix} -1 & 2 & 2 \\ 2 & -1 & 2 \\ 2 & 2 & -1 \end{pmatrix}$	$\begin{pmatrix} 1 & 0 & 0 \\ 0 & 0 & 1 \\ 0 & 1 & 0 \end{pmatrix}$
$\mathbf{3}'$	$\begin{pmatrix} 1 & 0 & 0 \\ 0 & \omega^2 & 0 \\ 0 & 0 & \omega \end{pmatrix}$	$\frac{1}{3} \begin{pmatrix} -1 & 2 & 2 \\ 2 & -1 & 2 \\ 2 & 2 & -1 \end{pmatrix}$	$-\begin{pmatrix} 1 & 0 & 0 \\ 0 & 0 & 1 \\ 0 & 1 & 0 \end{pmatrix}$

TABLE IV: The representation matrices for the S_4 generators T , S and U , where $\omega = e^{2\pi i/3}$.

for $a, b \sim \mathbf{3}$ or $a, b \sim \mathbf{3}'$, and

$$\begin{aligned}
(ab)_{\mathbf{1}'} &= a_1 b_1 + a_2 b_3 + a_3 b_2, \\
(ab)_{\mathbf{2}} &= (a_2 b_2 + a_1 b_3 + a_3 b_1, -(a_3 b_3 + a_1 b_2 + a_2 b_1))^T, \\
(ab)_{\mathbf{3}'} &= (2a_1 b_1 - a_2 b_3 - a_3 b_2, 2a_3 b_3 - a_1 b_2 - a_2 b_1, 2a_2 b_2 - a_3 b_1 - a_1 b_3)^T, \\
(ab)_{\mathbf{3}} &= (a_2 b_3 - a_3 b_2, a_1 b_2 - a_2 b_1, a_3 b_1 - a_1 b_3)^T,
\end{aligned} \tag{A3}$$

for $a \sim \mathbf{3}$ or $b \sim \mathbf{3}'$. Contractions of a triplet $a = (a_1, a_2, a_3)^T \sim \mathbf{3}'$ and doublet $b = (b_1, b_2)^T \sim \mathbf{2}$ are given by

$$\begin{aligned}
(ab)_{\mathbf{3}'} &= (a_2 b_1 + a_3 b_2, a_3 b_1 + a_1 b_2, a_1 b_1 + a_2 b_2)^T, \\
(ab)_{\mathbf{3}} &= (a_2 b_1 - a_3 b_2, a_3 b_1 - a_1 b_2, a_1 b_1 - a_2 b_2)^T,
\end{aligned} \tag{A4}$$

Lagrangian terms contributing to lepton masses and invariant under $S_4 \times Z_4$ are given by

$$\begin{aligned}
-\mathcal{L} \supset & \frac{y_{e1}}{\Lambda^3} (\bar{L}(\varphi\varphi)_{\mathbf{2}})_{\mathbf{3}} \mathbf{1} H e_R + \frac{y_{e2}}{\Lambda^3} (\bar{L}(\varphi\varphi)_{\mathbf{3}})_{\mathbf{3}} \mathbf{1} H e_R + \frac{y_{\mu}}{2\Lambda^2} (\bar{L}(\varphi\varphi)_{\mathbf{3}})_{\mathbf{1}} H \mu_R + \frac{y_{\tau}}{\Lambda} (\bar{L}\varphi)_{\mathbf{1}'} H \tau_R \\
& + \frac{\tilde{H}\tilde{H}}{2\Lambda_{ss}\Lambda} \left[y_1 (\bar{L}L^c)_{\mathbf{1}} \xi + y_2 ((\bar{L}L^c)_{\mathbf{2}} \zeta)_{\mathbf{2}} + y_3 ((\bar{L}L^c)_{\mathbf{3}} \chi)_{\mathbf{3}} \right] + \text{h.c.} .
\end{aligned} \tag{A5}$$

Applying the CG coefficients to the above formula, we arrive at Eq. (A5) with $y_e = -y_{e1} + 2y_{e2}$. With the help of the CG coefficient, Lagrangian terms contribute to NSI in Eq. (17) can be written in a more compact form,

$$-\mathcal{L} \supset \mu_{\eta}^2 (\tilde{\eta}\eta)_{\mathbf{1}} + \mu_{\phi}^2 \phi^{-} \phi^{+} + \left(f \phi^{-} \tilde{H}^{\dagger} (\eta\chi)_{\mathbf{1}} + \text{h.c.} \right) + \lambda (\bar{L}\eta)_{\mathbf{1}} e_R, \tag{A6}$$

where $\tilde{\eta} = (\eta_1^\dagger, \eta_3^\dagger, \eta_2^\dagger)$ is understood. They invariant under the symmetry $S_4 \times Z_4 \times Z_2$.

-
- [1] M. Tanabashi *et al.* (Particle Data Group), *Phys. Rev.* **D98**, 030001 (2018).
 - [2] T. Fukuyama and H. Nishiura, (1997), [arXiv:hep-ph/9702253 \[hep-ph\]](#); E. Ma and M. Raidal, *Phys. Rev. Lett.* **87**, 011802 (2001), [Erratum: *Phys. Rev. Lett.*87,159901(2001)], [arXiv:hep-ph/0102255 \[hep-ph\]](#); C. S. Lam, *Phys. Lett.* **B507**, 214 (2001), [arXiv:hep-ph/0104116 \[hep-ph\]](#); K. R. S. Balaji, W. Grimus, and T. Schwetz, *Phys. Lett.* **B508**, 301 (2001), [arXiv:hep-ph/0104035 \[hep-ph\]](#); P. F. Harrison, D. H. Perkins, and W. G. Scott, *Phys. Lett.* **B530**, 167 (2002), [arXiv:hep-ph/0202074 \[hep-ph\]](#).
 - [3] P. F. Harrison and W. G. Scott, *Phys. Lett.* **B547**, 219 (2002), [arXiv:hep-ph/0210197 \[hep-ph\]](#).
 - [4] Z.-z. Xing and Z.-h. Zhao, *Rept. Prog. Phys.* **79**, 076201 (2016), [arXiv:1512.04207 \[hep-ph\]](#).
 - [5] J. Liao, D. Marfatia, and K. Whisnant, *Phys. Rev.* **D87**, 013003 (2013), [arXiv:1205.6860 \[hep-ph\]](#).
 - [6] F. Capozzi, E. Lisi, A. Marrone, D. Montanino, and A. Palazzo, *Nucl. Phys.* **B908**, 218 (2016), [arXiv:1601.07777 \[hep-ph\]](#); I. Esteban, M. C. Gonzalez-Garcia, M. Maltoni, I. Martinez-Soler, and T. Schwetz, (2016), [arXiv:1611.01514 \[hep-ph\]](#); P. F. de Salas, D. V. Forero, C. A. Ternes, M. Tortola, and J. W. F. Valle, (2017), [arXiv:1708.01186 \[hep-ph\]](#); I. Esteban, M. C. Gonzalez-Garcia, A. Hernandez-Cabezudo, M. Maltoni, and T. Schwetz, *JHEP* **01**, 106 (2019), [arXiv:1811.05487 \[hep-ph\]](#).
 - [7] S. F. King and C. C. Nishi, (2018), [arXiv:1807.00023 \[hep-ph\]](#).
 - [8] S. F. King and Y.-L. Zhou, (2019), [arXiv:1901.06877 \[hep-ph\]](#).
 - [9] F. Feruglio, C. Hagedorn, and R. Ziegler, *JHEP* **1307**, 027 (2013), [arXiv:1211.5560 \[hep-ph\]](#).
 - [10] M. Holthausen, M. Lindner, and M. A. Schmidt, *JHEP* **1304**, 122 (2013), [arXiv:1211.6953 \[hep-ph\]](#).
 - [11] Y.-L. Zhou, (2014), [arXiv:1409.8600 \[hep-ph\]](#).
 - [12] G.-J. Ding, S. F. King, and A. J. Stuart, *JHEP* **12**, 006 (2013), [arXiv:1307.4212 \[hep-ph\]](#).
 - [13] G.-J. Ding, S. F. King, C. Luhn, and A. J. Stuart, *JHEP* **05**, 084 (2013), [arXiv:1303.6180 \[hep-ph\]](#).
 - [14] G.-J. Ding and Y.-L. Zhou, (2013), [arXiv:1312.5222 \[hep-ph\]](#); *JHEP* **1406**, 023 (2014), [arXiv:1404.0592 \[hep-ph\]](#).
 - [15] G.-J. Ding and S. F. King, *Phys.Rev.* **D89**, 093020 (2014), [arXiv:1403.5846 \[hep-ph\]](#).
 - [16] F. Feruglio, C. Hagedorn, and R. Ziegler, *Eur. Phys. J.* **C74**, 2753 (2014), [arXiv:1303.7178 \[hep-ph\]](#).
 - [17] C.-C. Li and G.-J. Ding, (2014), [arXiv:1408.0785 \[hep-ph\]](#).
 - [18] L. Wolfenstein, *Phys. Rev.* **D17**, 2369 (1978).

- [19] R. Acciarri *et al.* (DUNE), (2015), [arXiv:1512.06148 \[physics.ins-det\]](#).
- [20] K. Abe *et al.* (Hyper-Kamiokande), (2018), [arXiv:1805.04163 \[physics.ins-det\]](#).
- [21] T. Ohlsson, *Rept. Prog. Phys.* **76**, 044201 (2013), [arXiv:1209.2710 \[hep-ph\]](#); O. G. Miranda and H. Nunokawa, *New J. Phys.* **17**, 095002 (2015), [arXiv:1505.06254 \[hep-ph\]](#); Y. Farzan and M. Tortola, *Front.in Phys.* **6**, 10 (2018), [arXiv:1710.09360 \[hep-ph\]](#).
- [22] J. Liao, D. Marfatia, and K. Whisnant, *Phys. Rev.* **D93**, 093016 (2016), [arXiv:1601.00927 \[hep-ph\]](#); S. K. Agarwalla, S. S. Chatterjee, and A. Palazzo, *Phys. Lett.* **B762**, 64 (2016), [arXiv:1607.01745 \[hep-ph\]](#); M. Masud and P. Mehta, *Phys. Rev.* **D94**, 053007 (2016), [arXiv:1606.05662 \[hep-ph\]](#); M. Ghosh and O. Yasuda, *Phys. Rev.* **D96**, 013001 (2017), [arXiv:1702.06482 \[hep-ph\]](#); L. J. Flores, E. A. Garcés, and O. G. Miranda, *Phys. Rev.* **D98**, 035030 (2018), [arXiv:1806.07951 \[hep-ph\]](#); M. Masud, S. Roy, and P. Mehta, *Phys. Rev.* **D99**, 115032 (2019), [arXiv:1812.10290 \[hep-ph\]](#).
- [23] J. Liao, D. Marfatia, and K. Whisnant, *JHEP* **01**, 071 (2017), [arXiv:1612.01443 \[hep-ph\]](#).
- [24] P. Bakhti and Y. Farzan, *JHEP* **07**, 064 (2014), [arXiv:1403.0744 \[hep-ph\]](#); P. Coloma and T. Schwetz, *Phys. Rev.* **D94**, 055005 (2016), [arXiv:1604.05772 \[hep-ph\]](#); K. N. Deepthi, S. Goswami, and N. Nath, *Phys. Rev.* **D96**, 075023 (2017), [arXiv:1612.00784 \[hep-ph\]](#).
- [25] P. Coloma, *JHEP* **03**, 016 (2016), [arXiv:1511.06357 \[hep-ph\]](#); M. Masud, A. Chatterjee, and P. Mehta, *J. Phys.* **G43**, 095005 (2016), [arXiv:1510.08261 \[hep-ph\]](#); A. de Gouvêa and K. J. Kelly, *Nucl. Phys.* **B908**, 318 (2016), [arXiv:1511.05562 \[hep-ph\]](#); K. Huitu, T. J. Kärkkäinen, J. Maalampi, and S. Vihonen, *Phys. Rev.* **D93**, 053016 (2016), [arXiv:1601.07730 \[hep-ph\]](#); D. V. Forero and P. Huber, *Phys. Rev. Lett.* **117**, 031801 (2016), [arXiv:1601.03736 \[hep-ph\]](#); M. Masud and P. Mehta, *Phys. Rev.* **D94**, 013014 (2016), [arXiv:1603.01380 \[hep-ph\]](#); S.-F. Ge and A. Yu. Smirnov, *JHEP* **10**, 138 (2016), [arXiv:1607.08513 \[hep-ph\]](#); K. N. Deepthi, S. Goswami, and N. Nath, *Nucl. Phys.* **B936**, 91 (2018), [arXiv:1711.04840 \[hep-ph\]](#); F. Capozzi, S. S. Chatterjee, and A. Palazzo, (2019), [arXiv:1908.06992 \[hep-ph\]](#).
- [26] D. V. Forero and W.-C. Huang, *JHEP* **03**, 018 (2017), [arXiv:1608.04719 \[hep-ph\]](#); U. K. Dey, N. Nath, and S. Sadhukhan, *Phys. Rev.* **D98**, 055004 (2018), [arXiv:1804.05808 \[hep-ph\]](#).
- [27] T. Wang and Y.-L. Zhou, *Phys. Rev.* **D99**, 035039 (2019), [arXiv:1801.05656 \[hep-ph\]](#).
- [28] V. Barger, D. Marfatia, and K. Whisnant, *Phys. Rev.* **D65**, 073023 (2002), [arXiv:hep-ph/0112119 \[hep-ph\]](#).
- [29] T. Alion *et al.* (DUNE), (2016), [arXiv:1606.09550 \[physics.ins-det\]](#).
- [30] P. Huber, M. Lindner, and W. Winter, *Comput. Phys. Commun.* **167**, 195 (2005), [arXiv:hep-ph/0407333 \[hep-ph\]](#).
- [31] P. Huber, J. Kopp, M. Lindner, M. Rolinec, and W. Winter, *Comput. Phys. Commun.* **177**, 432 (2007), [arXiv:hep-ph/0701187 \[hep-ph\]](#).
- [32] J. Kopp, *Int. J. Mod. Phys.* **C19**, 523 (2008), [arXiv:physics/0610206 \[physics\]](#).
- [33] J. Kopp, M. Lindner, T. Ota, and J. Sato, *Phys. Rev.* **D77**, 013007 (2008), [arXiv:0708.0152](#)

[hep-ph].

- [34] P. Ballett, S. F. King, S. Pascoli, N. W. Prouse, and T. Wang, *Phys. Rev.* **D96**, 033003 (2017), [arXiv:1612.07275 \[hep-ph\]](#).
- [35] F. Bazzocchi, L. Merlo, and S. Morisi, *Nucl. Phys.* **B816**, 204 (2009), [arXiv:0901.2086 \[hep-ph\]](#).
- [36] G.-J. Ding and Y.-L. Zhou, *Nucl. Phys.* **B876**, 418 (2013), [arXiv:1304.2645 \[hep-ph\]](#).
- [37] I. de Medeiros Varzielas, T. Neder, and Y.-L. Zhou, *Phys. Rev.* **D97**, 115033 (2018), [arXiv:1711.05716 \[hep-ph\]](#).